Dynamic Measurement of Altered Chemical Messenger Secretion after Cellular Uptake of Nanoparticles Using Carbon−Fiber Microelectrode Amperometry

ARTICLE *in* ANALYTICAL CHEMISTRY · JUNE 2008

Impact Factor: 5.64 · DOI: 10.1021/ac800006y · Source: PubMed

4 AUTHORS, INCLUDING:

Bryce James Marquis
University of Arkansas for Medical Sciences
18 PUBLICATIONS **456** CITATIONS
SEE PROFILE

Christy Haynes
University of Minnesota Twin Cities
140 PUBLICATIONS **8,855** CITATIONS
SEE PROFILE

Anal. Chem. **2008,** *80,* 3431−3437

Dynamic Measurement of Altered Chemical Messenger Secretion after Cellular Uptake of Nanoparticles Using Carbon-Fiber Microelectrode Amperometry

Bryce J. Marquis, Adam D. McFarland,† Katherine L. Braun, and Christy L. Haynes*

Department of Chemistry, University of Minnesota, 207 Pleasant Street SE, Minneapolis, Minnesota 55455

In this work, carbon-fiber microelectrode amperometry is used to characterize serotonin exocytosis from murine peritoneal mast cells cocultured with fibroblasts in the presence of Au nanoparticles. In the case of mast cell exposure to 1 nM 28 nm diameter spherical Au nanoparticles, there is a decrease of greater than 30% in the number of successful granule transport and fusion events, greater than 30% increase in the rate of intragranular matrix expansion, and greater than 20% increase in the number of secreted serotonin molecules per granule. These results suggest that nanoparticles interrupt the dense-core biopolymer intragranular matrix and present the potential for systematic studies showing how exocytotic function is influenced by nanoparticle size, shape, and composition.

Nanoscale materials are facilitating novel biomedical applications in the areas of therapeutics and assay development. In particular, Au nanoparticles have found wide application, due to their ease of synthesis and facile surface chemistry modification,[1] in the areas of DNA and drug delivery,[2−5] direct inhibition of cancer cell proliferation,[6] photodynamic therapy,[7] and both intra- and extracellular biomarker probes.[1,8−12] Characterizing the basic interaction of these nanoparticles with biological cells is critical for data interpretation and further technological development. This characterization of nanoparticle−cell interaction suffers from a paucity of analytical chemistry studies and presents interesting measurement challenges based on the complex biological environment, the dynamic nature of the nanoparticle−cell interaction, and the high sensitivities required for single-cell assays.

The majority of current work studying engineered nanoparticle effects on cellular function exploits techniques traditionally used by toxicologists to study the influence of molecular species on cellular function, even though cell−nanoparticle interactions are likely to proceed by vastly different mechanisms. These techniques typically assess cellular viability through a variety of means, the vast majority of which measure mitochondrial activity using tetrazolium-based assays such as the MTT or WST-1 assay. Although understanding nanoparticle effects on mitochondrial activity is important, it is just one of many relevant cellular functions. Furthermore, a series of recent papers have revealed spurious results from these assays due to redox reactions between tetrazolium-based dyes and nanomaterials.[13] Other viability techniques include neutral red, trypan blue, and propidium iodide assays, all of which risk mischaracterization by reactions of the probe molecules with nanomaterials. Interpretation of all of the aforementioned assays is complicated by the ensemble-averaged nature of the data, often collected from millions of cells in order to achieve sufficient signal-to-noise ratios. Many cell lines must be cocultured with a support cell to simulate in vivo cell actions (as is done in the work presented herein); these traditional assays are incapable of distinguishing the target cell response from the support cell response, resulting in an ensemble-averaged measurement from multiple cell types, limiting interpretation possibilities. The data presented here address this limitation with direct, real-time amperometric measurements on individual immune system cells as they exocytose serotonin.

Recently, high-throughput cDNA microarray assays of nanoparticle-exposed cells have been performed, and initial data reveals both up-regulation and down-regulation of different classes of

* To whom correspondence should be addressed. E-mail: chaynes@umn.edu.

† Current address: Eli Lilly & Company, Indianapolis, IN 46285.

(1) Ho, K. C.; Tsai, P. J.; Lin, Y. S.; Chen, Y. C. *Anal. Chem.* **2004**, *76*, 7162−7168.
(2) Kogan, M. J.; Olmedo, I.; Hosta, L.; Guerrero, A. R.; Cruz, L. J.; Albericio, F. *Nanomedicine* **2007**, *2*, 287−306.
(3) Li, J.; Wang, X.; Wang, C.; Chen, B.; Dai, Y.; Zhang, R.; Song, M.; Lv, G.; Fu, D. *ChemMedChem* **2007**, *2*, 374−378.
(4) Bhattarai, S. R.; Remant, B. K. C.; Aryal, S.; Bhattarai, N.; Kim, S. Y.; Yi, H. K.; Hwang, P. H.; Kim, H. Y. *J. Nanopart. Res.* **2008**, *10*, 151−162.
(5) Rosi, N. L.; Giljohann, D. A.; Thaxton, C. S.; Lytton-Jean, A. K. R.; Han, M. S.; Mirkin, C. A. *Science* **2006**, *312*, 1027−1030.
(6) Bhattacharya, R.; Patra, C. R.; Verma, R.; Kumar, S.; Greipp, P. R.; Mukherjee, P. *Adv. Mater.* **2007**, *19*, 711−716.
(7) Paasonen, L.; Laaksonen, T.; Johans, C.; Yliperttula, M.; Kontturi, K.; Urth, A. *J. Controlled Release* **2007**, *122*, 86−93.
(8) Brusnichkin, A. V.; Nedosekin, D. A.; Proskurnin, M. A.; Zharov, V. P. *Appl. Spectrosc.* **2007**, *61*, 1191−1201.
(9) Lee, S.; Kim, S.; Choo, J.; Shin, S. Y.; Lee, Y. H.; Choi, H. Y.; Ha, S.; Kang, K.; Oh, C. H. *Anal. Chem.* **2007**, *79*, 916−922.
(10) Mishra, Y. K.; Mohapatra, S.; Avasthi, D. K.; Kabiraj, D.; Lalla, N. P.; Pivin, J. C.; Sharma, H.; Kar, R.; Singh, N. *Nanotechnology* **2007**, *18*, 345606/345601−345606/345605.
(11) Shi, X.; Wang, S.; Meshinchi, S.; Van Antwerp, M. E.; Bi, X.; Lee, I.; Baker, J. R., Jr. *Small* **2007**, *3*, 1245−1252.
(12) Yu, C. X.; Nakshatri, H.; Irudayaraj, J. *Nano Lett.* **2007**, *7*, 2300−2306.
(13) Laaksonen, T.; Santos, H.; Vihola, H.; Salonen, J.; Riikonen, J.; Heikkila, T.; Peltonen, L.; Kumar, N.; Murzin, D. Y.; Lehto, V.-P.; Hirvonen, J. *Chem. Res. Toxicol.* **2007**, *20*, 1913−1918.

10.1021/ac800006y CCC: $40.75
Published on Web 03/15/2008

genes, including genes involved in signal transduction.[14,15] The effect of these alterations cannot be assessed without direct measurement of cellular communication after nanoparticle exposure. In this work, carbon-fiber microelectrode amperometry is implemented to measure the dynamic secretion of chemical messenger molecules from nanoparticle-exposed cells. This method facilitates detection of a specific molecular target based on applied potential, submillisecond time resolution, and quantitation of endogenous concentrations of chemical messengers released during exocytosis. Carbon-fiber microelectrode amperometry has been used previously to characterize exocytosis of serotonin (an electroactive chemical messenger) from primary cultured murine peritoneal mast cells, the model cells used in this work. These cells are known for their critical role in immune response and physiological protection against pathogens by the secretion of chemical messengers including histamine, serotonin, proteoglycans, proteases, leukotrienes, prostaglandins, and a myriad of cytokines into the interstitium as the dense core of the mast cell granules, composed of a negatively charged sulfated proteoglycan matrix, expands in an ion-exchange-driven process.[16] Although the experiments herein measure one chemical messenger molecule being delivered from one cell type, the process of granule-mediated chemical messenger delivery is critical to nearly all physiological processes and occurs in cell types such as neuronal, neuroendocrine, endocrine, exocrine, and homeopoietic cells. Any abnormality in the ability of these cells to deliver chemical messengers may present significant physiological ramifications.

A granule inside a mast cell undergoes five discrete steps that culminate in secretion,[17] any of which is susceptible to perturbation by internalized nanoparticles. First, granules are mobilized to the release zone via the actin−myosin cytoskeletal system.[18] Second, the granules dock in the release zone either through the formation of the SNARE complex[19] or interaction with Sec1/Munc18 (SM) proteins.[20] Third, in an ATP-dependent priming step, a conformation change of the SNARE and/or SM protein complex makes the docked granule fusion competent.[21] Fourth, high intracellular Ca^{2+} concentrations trigger a SNARE complex conformation change that drives fusion of the granule and intracellular lipid bilayers.[22] Finally, the intravesicular matrix expands and expels the granule contents into the extracellular space.[18] Although the aforementioned cytoskeletal elements and proteins are specific to mast cells, most exocytotic cells follow a similar scheme, making mast cell secretion of serotonin a good model for assessing the effect of nanoscale materials on this critical cell behavior.

EXPERIMENTAL SECTION

Nanoparticle Synthesis. All glassware was cleaned with aqua regia (3:1 HCl/HNO_3) and rinsed before use in nanoparticle synthesis. Citrate-reduced Au colloids were synthesized by the addition of 60.2 μL of 30% hydrogen tetrachloroaurate (Sigma Aldrich, Milwaukee, WI) to 10 mL of a 4.0 mM sodium citrate solution (Sigma Aldrich, Milwaukee, WI), followed by sonication for 30 min in a nitrogen environment. This preparation yields a dark purple solution with an extinction maximum at 542.6 nm and an optical density of 0.344 (9:1 dilution) and, thus, a concentration of 12.9 nM nanoparticles. These nanoparticles were then dialyzed in cellulose dialysis tubing (Fisher Scientific, Waltham, MA) against filtered deionized water (Millipore, Billerica, MA) for 96 h, replacing the water outside the dialysis membrane every 24 h. The resultant dialyzed colloids have an extinction maximum of 544.2 nm and an optical density of 0.200 (9:1 dilution) and, thus, a concentration of 9.0 nM nanoparticles using a previously published extinction coefficient for 28 nm diameter spherical Au colloids.[23] Both dialyzed and nondialyzed colloids were deposited onto Formvar-coated copper grids (Electron Microscopy Sciences, Hatfield, PA) and characterized by transmission electron microscopy (TEM) with a JEOL JEM 1210 (JEOL, Tokyo, Japan) at 120 kV accelerating voltage.

Cell Culture. 3t3 Swiss-albino fibroblasts were obtained from American Type Tissue Collection (Manassas, VA) and grown in Dulbecco's modified Eagle's media (HyClone, Logan, UT) formulated with 4.5 mM L-glutamine, 4.5 mg/mL L-glucose, 110 mg/mL sodium pyruvate and supplemented with 10% bovine calf serum (Sigma Aldrich, Milwaukee, WI) and 10 U/mL penicillin and 10 mg/mL streptomycin (Gibco, Carlsbad, CA). Fibroblasts were plated on 35 mm Petri dishes and grown to confluence in an incubator held at 37 °C and 5% CO_2, changing media every 2 days.

Mast cells were obtained by peritoneal lavage. Briefly, 5 mL of cold growth media was injected into the peritoneal cavity of C57BL/6J mice (Jackson labs, Bar Harbor, ME) immediately following euthanasia by CO_2 asphyxiation according to protocol no. 0509A75006 approved by the University of Minnesota Institutional Animal Care and Use Committee. The peritoneal cavity was massaged for 2 min before removal of the lavage fluid. Cells were isolated from the lavage fluid by centrifugation at 300*g* for 5 min, resuspended in growth media, and plated at 1.5×10^5 cells/mL on top of confluent fibroblasts. Cells were allowed to stabilize for 1 h before exposure to experimental conditions. Experimental conditions included the premixing of nanoparticle solutions with culture media containing 10% bovine calf serum (to discourage nanoparticle aggregation[24]) to yield the desired concentration before replacement of growth media with experimental media. The nanoparticle concentration range was chosen based on previous viability studies that demonstrated that the presence of nanomolar Au does not cause cell death;[24,25] this is also the likely concentration range for human exposure to engineered nanopar-

(14) Chen, H. W.; Su, S. F.; Chien, C. T.; Lin, W. H.; Yu, S. L.; Chou, C. C.; Chen, J. J. W.; Yang, P. C. *FASEB J.* **2006**, *20*, 2393 ff.
(15) Fanqing, C. Toxicology and Cellular Effects of Manufactured Nanomaterials. European Patent WO2006US60369 20061030, 2007.
(16) Benoist, C.; Mathis, D. *Nature* **2002**, *420*, 875−878.
(17) Lin, R. C.; Scheller, R. H. *Annu. Rev. Cell Dev. Biol.* **2000**, *16*, 19−49.
(18) Wightman, R. M.; Schroeder, T. J.; Finnegan, J. M.; Ciolkowski, E. L.; Pihel, K. *Biophys. J.* **1995**, *68*, 383−390.
(19) Sollner, T.; Bennett, M. K.; Whiteheart, S. W.; Scheller, R. H.; Rothman, J. E. *Cell* **1993**, *75*, 409−418.
(20) Toonen, R. F. G.; Verhage, M. *Trends Cell Biol.* **2003**, *13*, 177−186.
(21) Bittner, M. A.; Holz, R. W. *J. Biol. Chem.* **1992**, *267*, 16226−16229.
(22) Chen, Y. A.; Scales, S. J.; Patel, S. M.; Doung, Y. C.; Scheller, R. H. *Cell* **1999**, *97*, 165−174.
(23) Jensen, T. R.; Malinsky, M. D.; Haynes, C. L.; Van Duyne, R. P. *J. Phys. Chem. B* **2000**, *104*, 10549−10556.
(24) Chithrani, B. D.; Ghazani, A. A.; Chan, W. C. W. *Nano Lett.* **2006**, *6*, 662−668.
(25) Connor, E. E.; Mwamuka, J.; Gole, A.; Murphy, C. J.; Wyatt, M. D. *Small* **2005**, *1*, 325−327.

ticles.[26] For control conditions, culture media was diluted with sterile water to match the amount of nanoparticle solution added for the most concentrated exposure to account for possible media dilution effects. Experimental media was refreshed every 24 h with media matching initial experimental conditions. Tris buffer solution was prepared with a final osmolarity of 335.2 mOsm including 300 mM sodium chloride, 12.5 mM trishydroxymethylaminomethane, 8.4 mM potassium chloride, 5.6 mM α-D-glucose, 4.5 mM calcium chloride, and 4.2 mM magnesium chloride. Cell media was replaced with warm Tris buffer immediately before amperometry experiments.

Transmission Electron Microscopy. Cells were harvested and cultured as previously described. Cells to be prepared for TEM were removed by vigorous washing with phosphate-buffered saline (pH 7.4) and collected via centrifugation (5 min at 300*g*). After washing three times with cacodylate buffer (pH 7.4), cells were placed in a primary fixation solution of 2.5% glutaraldehyde (Sigma Aldrich, Milwaukee, WI) in cacodylate buffer at room temperature for 1 h. Cells were then postfixed with 1% osmium tetroxide (Sigma Aldrich, Milwaukee, WI) in cacodylate buffer at room temperature for 1 h. Dehydration was accomplished by immersing the cell pellet in increasing concentrations of ethanol in water (50%, 70%, 80%, 95%, and 100% ethanol, 5 min each). This procedure was repeated, replacing ethanol with propylene oxide (same volume percents and time as previous step). Cells were then infiltrated with 50:50 propylene oxide/Epon and placed into a desiccator. The infiltration mixture was replaced with fresh mixture after 2, 12, 24, and 48 h and then placed in an oven at 60 °C for 24 h. After the resin had fully cured, the sample was cut into 60 nm thick sections using a diamond knife (Delaware Diamond Knives, Inc., Wilmington, DE) on an ultramicrotome (Reichert, Wien, Austria). These sections were collected on Formvar-coated TEM grids (Electron Microscopy Sciences, Hatfield, PA) and stained with uranyl acetate and lead citrate (Sigma Aldrich, Milwaukee, WI). Sections were imaged using a JEOL JEM-1200 EXII TEM (JEOL, Tokyo, Japan) at an accelerating voltage of 60 kV.

Carbon-Fiber Microelectrode Amperometry. Electrodes were constructed following a previously published method. Briefly, a 4−6 in. long graphite fiber (Amoco, Greenville, SC) was aspirated into a glass capillary of 1.2 mm o.d. and 0.68 mm i.d. (A-M Systems, Carlsborg, WA). The filled capillary was then resistively heated and pulled using a micropipette puller (Narishige, Tokyo, Japan). Carbon fibers protruding from the end of the pulled capillary were then cut to a length of less than 10 μm. The microelectrode was then back-filled with a freshly prepared mixture of 15% (w/w) 1,3-pheylenediamine (Sigma Aldrich, Milwaukee, WI) in Epon resin 828 (Miller-Stephenson, Morton Grove, IL) for 30 s. The microelectrodes cured at room temperature for 24 h, then at 100 °C for 24 h, and finally, at 150 °C for an additional 24 h. Before use, microelectrode tips were beveled at 45° using a diamond polishing wheel (Sutter Instruments, Novato, CA) and stored in filtered isopropyl alcohol. Electrodes were back-filled with a 3.0 M potassium acetate/30.0 mM potassium chloride solution to provide electrical continuity to the potentiostat headstage electronics. Before each single-cell measurement, microelectrodes were pretreated by cycling an applied voltage between 0 and +1.4 V (vs a Ag/AgCl reference electrode) for 30 s at 400 V/s in a 0.1 M NaOH aqueous solution.

Micropipettes for the delivery of the secretagogue solution were made using the aforementioned capillary material. In this case, empty capillaries were pulled. Micropipettes with tip openings of 15−20 μm and smooth edges were chosen to produce a smooth secretagogue trajectory. Micropipettes were loaded with 5 μM A23187 (Sigma Aldrich, Milwaukee, WI) and connected to a Picospritzer III (Parker Hannifin, Cleveland, OH) for secretagogue ejection.

Amperometry experiments were conducted on an inverted TE-2000 microscope (Nikon U.S.A., Melville, NY) with phase contrast optics. Burleigh PCS-500 piezoelectric micromanipulators (Olympus America Inc., Center Valley, PA) were used for fine positioning of the electrode and the stimulation micropipette. Detected current is filtered using a low-pass Bessel filter (5 kHz) and amplified with gain of 10−20 mV/pA through an Axon Instruments Axopatch 200B (Molecular Devices, Inc., Sunnyvale, CA). Experimental parameter control and data acquisition were accomplished using a home-built breakout box and custom software modules created using the LabVIEW (National Instruments, Austin, TX) programming language.

In a typical amperometry experiment, growth media was removed from mast cell plates after 48 h exposure to experimental conditions, washed twice, and filled with Tris buffer solution (pH 7.4, 37 °C). During the course of the experiment, the cell plate was held at 37 °C using a temperature-control stage (Warner Inst., Hamden, CT). The microelectrode, micropipette, and reference electrode (Ag/AgCl) were lowered into the solution, and a voltage sufficient to oxidize serotonin (+700 mV vs Ag/AgCl) was applied to the microelectrode. Mast cells were selected based on their spherical shape, size (∼10−20 μm diameter), and the high contrast of their membrane that is observed when viewed with transmitted light microscopy. The microelectrode was lowered into contact with a mast cell, and the micropipette was placed 20−100 μm from the cell. A 3 s bolus of stimulation solution was delivered to the target mast cell, projected by a 1−3 psi nitrogen pulse. Data acquisition began 3 s before the stimulation pulse and continued for 90 s. Electrodes were pretreated as previously described between every trace and were used a maximum of six times to minimize effects of serotonin fouling of the electrode surface. Experiments were conducted on individual cell culture plates for a maximum of 2 h, yielding between 5 and 15 individual cell traces per cell plate.

Data Analysis. Amperometric data was exported and analyzed using MiniAnalysis software (Synaptosoft Inc., Fort Lee, NJ). The spike detection threshold was set to 5 times the root-mean-square current noise, and the minimum spike area was set to 70 fC. On the basis of the average $t_{1/2}$ of mast cell amperometric spikes (∼14 ms), an interspike interval of less than ∼7 ms could cause two individual spikes to be mistakenly analyzed as a single degranulation event under the most conservative estimate. Analysis of the interspike intervals for mast cells reveal that the average interspike interval (measured from apex to apex) is 470 ms and only 0.31% of the measured spike intervals are 7 ms or less. On the basis of the time resolution of the amperometric measurement (0.05 ms) and this low probability, the analysis presented herein assumes

(26) Oberdorster, G.; Oberdorster, E.; Oberdorster, J. *Environ. Health Perspect.* **2005**, *113*, 823−839.

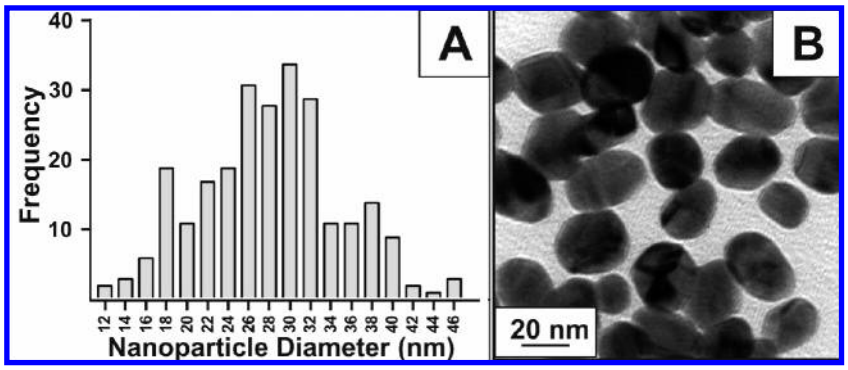

Figure 1. (A) Histogram showing the size distribution of the Au nanoparticles used in this work based on transmission electron microscopy (TEM) studies with 120 kV accelerating voltage. (B) TEM image of typical Au colloids used in toxicity experiments ($n = 250$).

that each spike represents an individual degranulation event. Mean values for the spike characteristics in each trace are combined among cells treated with the same experimental conditions and averaged to provide mean experimental values. Spike frequency is an exception to this procedure because each trace yields a single value that was then averaged over the series of cells. In all cases, $n \geq 11$ cells. To minimize bias toward larger values when removing outliers, logarithms of standard deviations and experimental means were taken, and logged experimental values more than two logged standard deviations from the log mean were considered statistical outliers. The significant differences between control and nanoparticle-exposed cells were determined using a two-tailed Student's t test assuming equal sample variances ($\alpha = 0.05$) using Microsoft Excel's data analysis toolkit (Microsoft Inc., Seattle, WA).

Foot analysis was performed using a subroutine in the MiniAnalysis software. First, all spikes with a foot feature were identified manually. Then, the baseline, apex, and inflection point between the foot and the full fusion spike were identified. After an exponential fit to the spike's decay curve, the area of both the foot and the spike portions of the event were calculated. In this work, only foot events that were followed directly by a full fusion spike were included. Similar to the interspike interval analysis done above, as well as that done in previous work,[27] it is possible to statistically assess the likelihood that an identified foot-spike event is actually two coincident spikes. In this case, an interspike interval of 14 ms or less could result in the misidentification of two nearly coincident spikes as a foot-spike combination. In fact, only 0.71% of the interspike intervals are 14 ms or less, and thus, there is approximately a 7-fold difference between the number of spikes that could be misidentified as a foot-spike combination and the actual number of feet detected.

RESULTS AND DISCUSSION

Herein, the advantages of using single-cell amperometry to probe nanoparticle−cell interaction are demonstrated using mast cells exposed to nanomolar concentrations of serum-coated Au nanoparticles. These nanoparticles were synthesized through sonication-initiated sodium citrate reduction of a Au^{3+} salt, dialyzed against buffer to eliminate chemical precursors, and suspended in serum-containing media; TEM analysis shows spherical Au

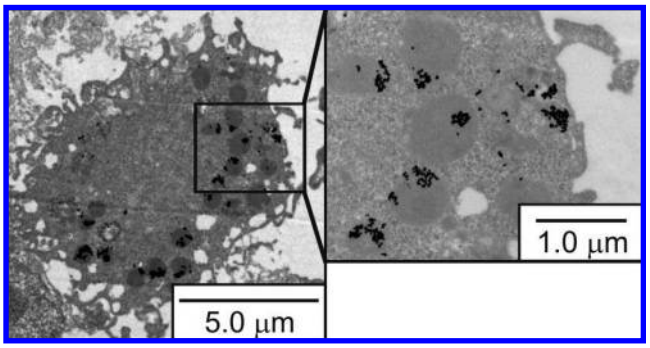

Figure 2. (Left) TEM image (7500×) of a murine peritoneal mast cell exposed to 1.0 nM 28.1 ± 6.7 nm diameter Au colloids for 48 h; (right) magnified image (25 000×) of the boxed region showing the location of nanoparticles within the mast cell. Au nanoparticles are localized most prevalently within the granules, but there are also nanoparticles within the cytoplasm. Both agglomerated clusters and isolated nanoparticles are apparent.

nanoparticles with a diameter of 28.1 ± 6.7 nm (Figure 1). Upon incubating mast cells with the aforementioned Au nanoparticles, TEM images reveal that the mast cells take up the Au nanoparticles (Figure 2) and that the nanoparticles agglomerate to a small degree within the granular matrix. Often, the nanoparticles are found localized on or inside the secretory granules. Both cellular and granular nanoparticle loading appears heterogeneous by TEM. Other cell types in culture, including fibroblasts, macrophages, lymphocytes, and granulocytes, were also found to take up nanoparticles and localize a majority of them in granular bodies (Figure 3). Statistical analysis of nanoparticle concentration- and time-dependent loading of mast cells is the subject of future work though literature precedent suggests that both increased concentration and exposure time lead to increased nanoparticle uptake until a threshold loading is reached.

With the knowledge that the serum-coated Au nanoparticles are taken up into mast cells, single-cell amperometry experiments were initiated to compare the dynamic process of serotonin exocytosis from cells exposed to various nanoparticle concentrations for 48 h. In this work, individual mast cells were stimulated to exocytose using a Ca^{2+} ionophore, and only serotonin secretion was measured; although electroactive histamine is simultaneously released from mast cell granules, it is oxidized at much higher potentials than serotonin and thus can be neglected here.[28] The

(27) Haynes, C. L.; Siff, L. N.; Wightman, R. M. *Biochim. Biophys. Acta* **2007**, *1773*, 728−735.

(28) Sarada, B. V.; Rao, T. N.; Tryk, D. A.; Fujishima, A. *Anal. Chem.* **2000**, *72*, 1632−1638.

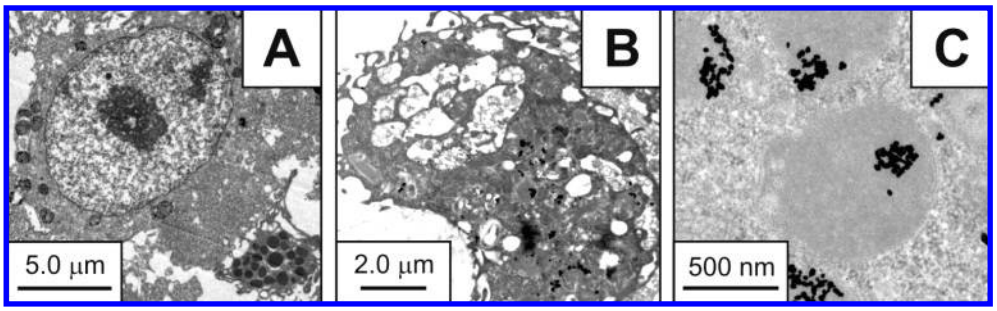

Figure 3. TEM images of cells exposed to 1.0 nM 28.1 ± 6.7 nm diameter Au nanoparticles for 48 h. (A) TEM image of a leukocyte (center) with significant nanoparticle loading within granular bodies; in the bottom right a section of a mast cell without significant nanoparticle loading is visible. The dark regions in the mast cell are the granule dense-core matrixes; this is verified by examining the crystallinity at higher magnifications. (B) Image of a macrophage with nanoparticle loading in both cytoplasm and granular bodies. (C) High-magnification TEM of granular bodies found in a leukocyte loaded with nanoparticles; the characteristic granular-limiting membrane is resolved.

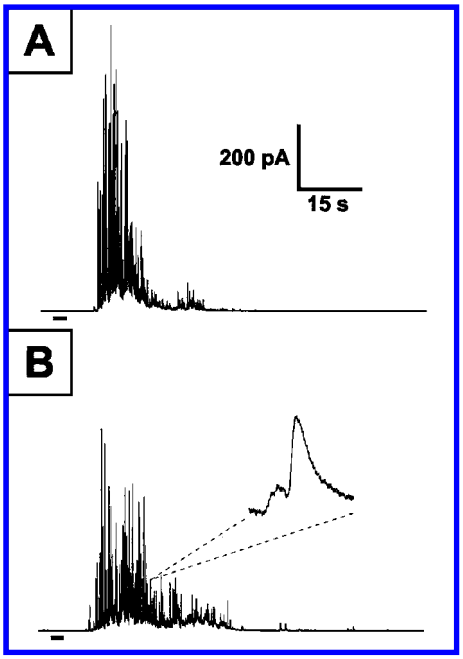

Figure 4. Representative amperometric traces of degranulation events from stimulated mast cells (A) exposed to 1.0 nM 28.1 ± 6.7 nm diameter Au colloids for 48 h and (B) control plates. The 3 s secretagogue stimulation pulse is indicated by the bold line below each trace. The lower inset displays an expanded view of an individual amperometric spike including a prespike foot event.

exocytosis events are monitored when a 7 μm diameter carbon-fiber microelectrode held at +700 mV versus the Ag/AgCl reference electrode, a potential sufficient to oxidize serotonin, is placed in contact with the mast cell membrane. The serotonin content of each granule is recorded as a current spike (Figure 4). Analysis of amperometric spike characteristics reveals rich details about the secretory granule's intracellular movement toward the cell membrane, fusion with the cell membrane, and ion exchange between the extracellular buffer and the intragranular matrix. The correlation between amperometric trace characteristics and granule properties/behavior are well-established.[29] For each amperometric trace, the average spike area (Q), width at half-height ($t_{1/2}$), and frequency of spikes can be determined. The area under a spike can be directly related to the number of molecules secreted by using Faraday's law, $Q = nFm$, where Q is the charge, n is the number of electrons lost in the oxidation, F is Faraday's constant, and m is the number of moles of serotonin secreted. The $t_{1/2}$ value is a measure of the rate of expulsion of chemical messengers via ion exchange following cell−granule fusion. The direct interpretation of $t_{1/2}$ variations as intragranular polymer matrix effects has been clearly demonstrated in experiments where alterations in extracellular buffer pH and osmolarity influence the amperometric spike $t_{1/2}$.[30] Spike frequency reveals the number of granules that successfully fuse with the cell membrane to initiate exocytosis. A minority of amperometric events (usually 5−10%) are preceded by a prespike feature, also known as a foot (Figure 4 inset). The foot reveals an arrested state of granule−cell membrane fusion where vesicle contents leak through a small (viz., 5 nm) fusion pore.[31]

Upon analyzing the amperometric spike characteristics from mast cells exposed to Au nanoparticles of varying concentration (0, 0.01, 0.1, and 1.0 nM) for 48 h, significant trends in cell function changes are revealed (Figure 5). There is no significant change in Q, as compared to control cells, with exposure to 0.01 and 0.1 nM Au nanoparticles based on pairwise t tests; however, with exposure to 1.0 nM Au nanoparticles, Q increases from 1500 ± 100 to 2000 ± 100 fC. This indicates an increased exocytosis of 4.6×10^6 serotonin molecules per granule when 1 nM Au nanoparticles are added to the cellular environment ($p < 0.001$). Analysis of the spike $t_{1/2}$ characteristics demonstrates that, not only are more serotonin molecules being released in the presence of nanoparticles, but the exocytotic event is occurring faster than in unexposed cells. In control cells, the average ion-exchange-driven process of intragranular matrix expansion and secretion proceeds in 14.5 ± 0.7 ms while in cells exposed to 1.0 nM Au nanoparticles, the average $t_{1/2}$ is 9.7 ± 0.5 ms. The coincident increase in granule Q and decrease in granule $t_{1/2}$ suggest that the nanoparticle uptake, as visualized by TEM, disrupts the biopolymer matrix responsible for storing and releasing mast cell chemical messengers and that this disruption increases as the nanoparticle loading scales with incubation concentration.[24]

In further analysis, amperometric spike frequency decreases with increasing nanoparticle concentration from 3.22 ± 0.34 Hz for control cells to 2.13 ± 0.29 Hz for cell exposed to 1 nM Au

(29) Mosharov, E. V.; Sulzer, D. *Nat. Methods* **2005**, *2*, 651−658.

(30) Troyer, K. P.; Wightman, R. M. *J. Biol. Chem.* **2002**, *277*, 29101−29107.

(31) Amatore, C.; Arbault, S.; Bonifas, I.; Bouret, Y.; Erard, M.; Ewing, A. G.; Sombers, L. A. *Biophys. J.* **2005**, *88*, 4411−4420.

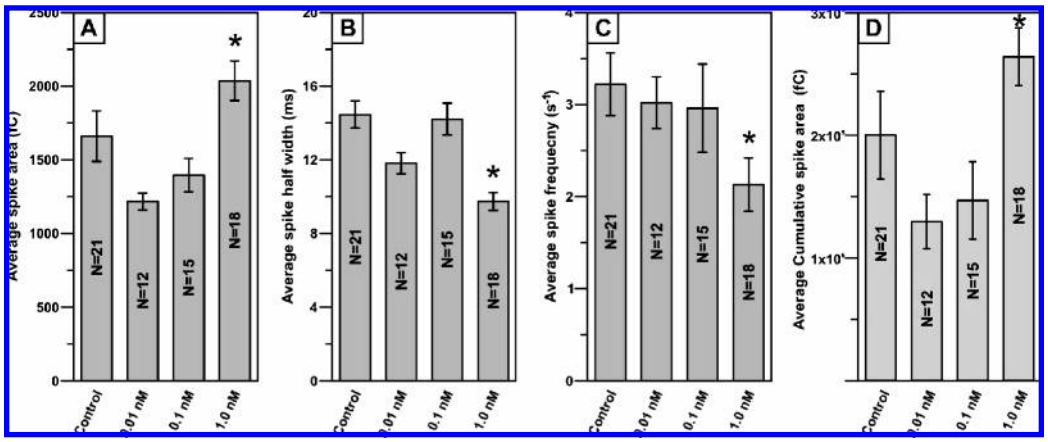

Figure 5. Gold nanoparticle concentration-dependent perturbation of exocytosis function in murine peritoneal mast cells: (A) average spike area increases with 1.0 nM Au nanoparticle exposure; (B) average spike half-width decreases with 1.0 nM Au nanoparticle exposure; (C) average spike frequency decreases with 1.0 nM Au nanoparticle exposure; (D) decrease in spike frequency with Au nanoparticle exposure does not result in an overall decrease in detected serotonin release per cell as demonstrated by the cumulative spike area increasing with 1.0 nM Au nanoparticle exposure. Error bars represent ±SEM, *n* values are shown on data bars, and ∗ indicates $p < 0.05$ in the *t* test.

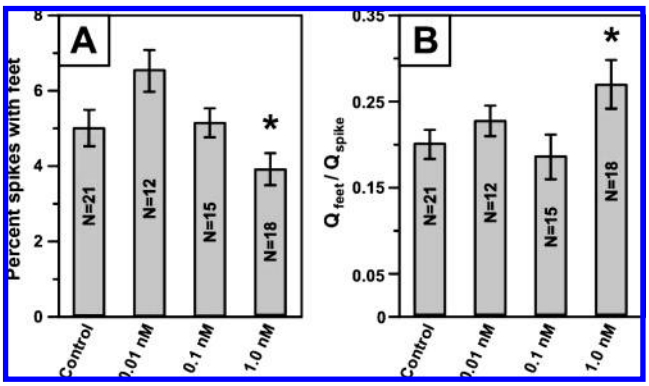

Figure 6. Gold nanoparticle concentration-dependent perturbation of prespike foot characteristics. (A) At high concentration exposure to Au nanoparticles, the number percentage of full fusion spikes that also demonstrate a prespike foot decreases relative to that of the control. (B) The ratio of the prespike foot area to the spike area increases with cell exposure to 1.0 nM Au nanoparticles. Error bars represent ±SEM, *n* values are shown on data bars, and ∗ indicates $p < 0.05$ in the *t* test.

nanoparticles. This decrease in spike frequency reveals that the nanoparticle presence also interferes with the cellular transport, docking, or fusion machinery. It is noteworthy that, although the frequency of spikes diminishes with increased nanoparticle exposure, the cumulative number of serotonin molecules released upon stimulation of an individual mast cell increases by an average of 1.65×10^8 molecules upon addition of 1.0 nM Au nanoparticles (Figure 5D, $p < 0.02$). Because the decreased frequency does not offset the synergistic influence of increased Q and decreased $t_{1/2}$, the nanoparticles' influence on the intragranular matrix is apparently larger than their influence on the transport/docking/fusion machinery.

Inspection of the prespike foot characteristics as a function of increased Au nanoparticle concentration (Figure 6) reveals a decrease in the percentage of spikes that display a prespike foot from 4.86% in control cells to 3.78% in 1 nM Au nanoparticle-exposed cells. This data suggests that the presence of nanoparticles interferes with the balance between granular membrane tension and biopolymer matrix expansion, the driving forces for fusion pore formation and sustenance. Foot characteristic analysis also reveals an increase in the relative number of molecules released during a fusion pore event, as compared to the following full fusion event, from 19.9% in control cells to 26.7% in 1 nM Au nanoparticle-exposed cells. The number of serotonin molecules released during a fusion pore opening must be considered relative to the number of serotonin molecules released during the corresponding full fusion to account for the known variability in granule volume within mast cells.[32] The significant increase in serotonin molecules released through the fusion pore when the highest concentration of nanoparticles is present further supports the aforementioned Q and $t_{1/2}$ trends where the nanoparticles alter serotonin storage in the intragranular biopolymer matrix.

CONCLUSION

With the use of carbon-fiber microelectrode amperometry combined with statistical analysis, altered exocytosis was detected and characterized from primary culture murine mast cells after 48 h of exposure to Au nanoparticles. This cell is a good model based on its extensive expression throughout the human immune system and the highly conserved nature of chemical messenger delivery machinery, even in cell types that do not secrete electroactive species and, thus, cannot be studied using single-cell amperometry. Unlike most analysis methods used to evaluate cell competence following nanoparticle exposure, amperometry is capable of real-time, dynamic detection of chemical messengers at the single-granule level. The work presented herein demonstrates that Au nanoparticle presence influences the number of chemical messenger molecules released as well as the rate and frequency at which they are released. Furthermore, this analysis also reveals changes in the balance between membrane surface tension and granular matrix expansion through prespike foot analysis. Overall, this work demonstrates the utility of microelectrode amperometry for analysis of engineered nanomaterial effects on exocytotic function. The real-time mechanistic details revealed by this functional assay fill an important gap between the large-scale screening done with traditional viability assays and the static

(32) Hammel, I.; Lagunoff, D.; Bauza, M.; Chi, E. *Cell Tissue Res.* **1983**, *228*, 51−59.

biomarker analysis accomplished with genotoxicity studies. Future work is required to elucidate the degree and mechanism of nanoparticle uptake as well as the mode of action resulting in the observed effects. However, it is clear that this method will be useful for identifying how nanoparticle material, size, shape, surface chemistry, and concentration influence cellular behavior, critical information as nanoparticle applications in therapeutics and cellular assays continue to expand.

ACKNOWLEDGMENT

We gratefully acknowledge Alice Ressler, an electron microscopy specialist at the University of Minnesota, for her assistance in developing and performing the TEM sample preparation. All electron microscopy work was carried out in the Institute of Technology Characterization Facility, University of Minnesota, which receives partial support from NSF through the NNIN program. We also acknowledge Professor Desmond J. Tobin for his assistance in expert identification of mast cells and mast cell granules in electron micrographs. Financial support for this work was generously provided by a 3M Non-Tenured Faculty Grant to C.L.H. and the National Science Foundation (No. CHE-0645041).

Received for review January 2, 2008. Accepted February 12, 2008.

AC800006Y